AGU PUBLICATIONS

Geophysical Research Letters

RESEARCH LETTER
10.1002/2017GL073603

Key Points:
- Permeability of mixed-wet rock to a fluid is enhanced by the presence of a second, stationary fluid
- The flowing phase need not be the nonwetting phase for enhanced permeability to occur in mixed-wet rock
- Equivalent slip lengths were <200 nm and decreased with increasing pore size

Supporting Information:
- Supporting Information S1

Correspondence to:
Y. Tanino,
ytanino@abdn.ac.uk

Citation:
Christensen, M., and Y. Tanino (2017), Enhanced permeability due to apparent oil/brine slippage in limestone and its dependence on wettability, *Geophys. Res. Lett.*, *44*, 6116–6123, doi:10.1002/2017GL073603.

Received 24 MAR 2017
Accepted 10 JUN 2017
Accepted article online 14 JUN 2017
Published online 29 JUN 2017

Enhanced permeability due to apparent oil/brine slippage in limestone and its dependence on wettability

M. Christensen[1] **and Y. Tanino**[1]

[1]School of Engineering, University of Aberdeen, Aberdeen, UK

Abstract End point relative permeabilities were measured in three limestones with permeabilities ranging from 0.6 to 220 mD under five wettability states established by adding different organic acids, of similar molecular structure but different alkyl chain length, to the oil phase. The altered wettability corresponding to each oil/brine pair is characterized by their dynamic contact angle on a polished calcite substrate, θ_w, which varied between 50° and 150°. Saturation-normalized relative permeability to oil exceeds one at $\theta_w < 140°$ in all rock considered. The equivalent slip length, defined by modeling the porous medium as a capillary tube with the defending phase distributed as an annular film on the tube wall, was below 200 nm in all experiments. The results indicate that commonly used models of relative permeability, which assume that the maximum permeability is the single-phase permeability, underestimate oil displacement for a much wider range of contact angles than previously documented.

1. Introduction

By analogy with Darcy's law which is derived by temporally and spatially averaging the Navier-Stokes equation, the ability of a porous medium to conduct a fluid in the presence of a second fluid is typically characterized by a phase-specific permeability defined as

$$k_i = \mu_i u_i \left(\frac{dp_i}{dx} \right)^{-1}, \quad (1)$$

where (μ_i, u_i, p_i) are the dynamic viscosity, volumetric flow rate per unit bulk cross-sectional area, and the pressure of phase *i*, respectively, and *x* is the direction of mean flow. In the present paper, i = w and i = o denote the aqueous phase and the oil phase, respectively. Unlike absolute (single-phase) permeability *k*, $k_i (\geq 0)$ is saturation and saturation history specific.

In pore network simulators [e.g., *Valvatne and Blunt*, 2004; *Joekar-Niasar et al.*, 2008; *Ryazanov et al.*, 2010], commercial reservoir simulators, empirical models [e.g., *Honarpour et al.*, 1982; *Burdine*, 1953; *Lomeland et al.*, 2005], and special core analysis [e.g., *Jerauld*, 1997; *Al-Gharbi et al.*, 2007], it is assumed that k_i cannot exceed absolute permeability, i.e., that relative permeability, $k_{ri} = k_i/k$, is ≤ 1. However, a number of studies have reported relative permeabilities to the nonwetting phase greater than 1 [*Berg et al.*, 2008, and references therein]. *Berg et al.* [2008] present a large set of end point k_{ri} data on reservoir sandstone cores under different aging conditions which show that $k_{ro} > 1$ at connate water saturation in roughly half of the aged (presumed weakly water-wet) samples and a smaller fraction of the unaged (presumed strongly water-wet) samples. The relative permeability to brine at residual oil saturation, S_{or}, was less than $k_{rw}/(1 - S_{or})^2 < 1$ in all unaged samples and most aged samples but exceeded 1 in a few aged samples [*Berg et al.*, 2008]. The authors associate enhanced permeability with the presence of a thin [*O*(100–700) nm], immobile film of connate water on the grain surface which, through an unidentified molecular mechanism, gives rise to slip. Unfortunately, no further information is available on the wettability of the samples so the assumption that the flowing, bulk fluid must be the nonwetting phase for relative permeability to exceed 1 could not be validated. Indeed, in the present paper we show that enhanced oil permeability occurs even when the rock is predominantly oil wetting.

Correlations have been observed between slip and a number of properties including the roughness of the solid surface [*Choi and Kim*, 2006; *Joseph et al.*, 2006], the molecular weight of polymers and resins in the fluid [*Wang and Drda*, 1996; *Drda and Wang*, 1995; *Bäumchen and Jacobs*, 2010], the molecular interaction between

the solid and the fluid, e.g., hydrophobicity [*Lee et al.*, 2007; *Choi and Kim*, 2006; *Cottin-Bizonne et al.*, 2008], and the velocity and shear rate [*Churaev et al.*, 1984; *Thompson and Troian*, 1997; *Choi et al.*, 2003; *Yang*, 2006]. The diversity of the correlations suggests that there is more than one mechanism through which slip may occur. The aforementioned studies considered single-phase flow on uniform solid surfaces. Slip of one liquid in the presence of a second liquid, in contrast, has received less attention. Even less attention has been given to slip under heterogeneous wettability, such as is typical of oil reservoirs and nonaqueous phase liquid-contaminated soils, despite strong evidence that contact angle is the controlling parameter for slip *Huang et al.* [2008].

This paper presents laboratory measurements of oil permeability at initial oil saturation (after primary drainage) and brine permeability at residual oil saturation (after waterflood) of three mixed-wet limestones for five different oils. Mixed wettability was established systematically by adding different organic acids to the oil phase at identical concentrations. The contact angle dependence of the end point permeabilities and their variation between the different limestones are discussed. A simple capillary tube model is used to translate the enhanced permeability into apparent slip lengths, which are compared to the characteristic pore size and the kinetic diameter of the organic acids in the oil phase.

2. Experimental Method

Experiments were performed on Indiana (USA), Estaillades (Vaucluse, France), and Guiting (Cotswold, UK) limestone cores. The cores were 37.63 ± 0.07 mm in diameter and varied in length between $L = 65.77$ and 89.60 mm; their mean porosity and absolute permeability were $(\phi, k) = (0.150 \pm 0.006, 7.6 \pm 2.9$ mD), $(0.28 \pm 0.01, 175 \pm 46$ mD), and $(0.272 \pm 0.004, 1.2 \pm 0.6$ mD) for Indiana, Estaillades, and Guiting limestone, respectively (Table S1 in the supporting information). Calcite is the most abundant mineral in each rock, comprising 99% of Indiana limestone [*Tanino and Blunt*, 2013], 98% of Estaillades limestone (Weatherford Laboratories, East Grinstead), and 80% of Guiting limestone [*Gharbi and Blunt*, 2012]. All three rocks contain significant microporosity [e.g., *Tanino and Blunt*, 2012] and are naturally water wetting.

In all experiments, an aqueous solution of 5 wt % NaCl, 1 wt % KCl saturated with carbonate was used as both the connate water and floodwater [cf. *Tanino and Blunt*, 2012, 2013; *Christensen and Tanino*, 2017]. Five oils were considered: *n*-decane (Sigma-Aldrich, ≥99%) and 6.6×10^{-2} M solutions of cyclohexanecarboxylic acid (Sigma-Aldrich 98%), cyclohexanepropionic acid (99%), cyclohexanebutyric acid (99%), and cyclohexanepentanoic acid (98%) in *n*-decane. This set of organic acids renders calcite hydrophobic (oil wetting) in order of increasing alkyl chain length, yielding dynamic advancing contact angles of $\theta_w \approx 55°$, 110°, 125°, 135°, and 150°, respectively, on polished calcite surfaces for the same aqueous phase [*Christensen and Tanino*, 2017; *Wu et al.*, 2008]. In this paper, the subscript "w" denotes a contact angle defined through the brine; $\theta_o = 180° - \theta_w$ is the corresponding angle defined through the oil phase. (Note that the nomenclature differs from that of *Christensen and Tanino* [2017].) Basic properties of the fluids are summarized in Table S1. Of particular relevance to the present analysis, the viscosities of the oils are 80 to 83% of the brine viscosity [*Christensen and Tanino*, 2017].

2.1. Relative Permeability Measurements

The coreflood apparatus and procedure closely follow that of *Tanino and Blunt* [2012] and *Christensen and Tanino* [2017]. The cores were horizontal, and experiments were performed at ambient temperature and pressure. The key steps were as follows, with details in the supporting information (Text S1):

1. Each core was fully saturated with degassed brine, and k was measured.
2. The test oil was injected into the core at constant pressure to establish initial oil saturation, S_{oi}, using the porous plate method [cf. *Tanino and Blunt*, 2012].
3. The porous plate was removed, and the permeability to oil, $k_o(S_{oi})$, was measured.
4. Up to 100 pore volumes (pv) of degassed brine was injected at either constant pressure (*n*-decane/Guiting limestone waterfloods) or at constant Darcy velocity, U_w, until residual state was established.

S_{oi} and S_{or} were determined by mass balance. This paper is focused on the maximum achievable S_{oi}, which was $S_{oi} \geq 0.8$ (Table S2). All waterfloods using test oils containing organic acid, i.e., $\theta_w > 90°$, were performed with a single U_w over the duration of the waterflood because the flow rate dependence of two-phase flow is not fully established under mixed-wet conditions. Only waterflood relative permeabilities at capillary numbers

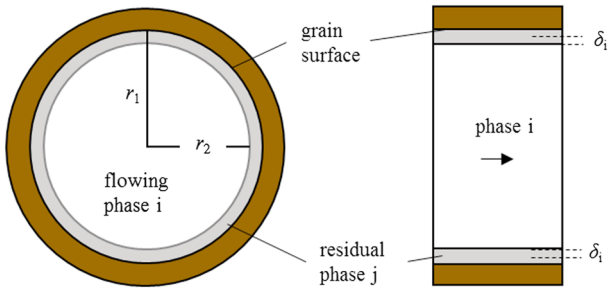

Figure 1. Schematic of (left) the cross section and (right) the diametral plane of a capillary tube of radius r_1, our model of the pore space in rock. The defending phase is distributed as an annular film of thickness $r_1 - r_2$ at the wall, and the injected phase flows through the middle of the tube.

below Ca $= \mu_w U_w/\sigma \leq 2 \times 10^{-7}$ are considered, where σ denotes interfacial tension; preliminary tests indicate that these values fall within the capillarity-dominated regime [*Tanino et al.*, 2015]. In addition, data from a coreflood performed by *Tanino and Blunt* [2012] is considered (TB/2); in this experiment the injection velocity was changed at discrete intervals. Pressures at the upstream and downstream ends of the core were measured throughout each experiment.

k and $k_o(S_{oi})$ were calculated from the steady state pressure drop across the core at three or four different flow rates as

$$k,\ k_i = \mu_i \frac{dU_i}{d(\Delta P_i/L)}, \tag{2}$$

where ΔP_i is the pressure drop across the core in injected phase i. Brine permeability at residual oil saturation, $k_w(S_{or})$, was determined using one of two methods. For 12 waterfloods, $k_w(S_{or})$ was estimated from ΔP_w after 100 pv of brine injection. In four waterfloods, brine was injected at three U_w or at three ΔP_w after S_{or} was established and, accordingly, $k_w(S_{or})$ was determined using equation (2). Where equation (2) was applied, the uncertainty in k and k_i is taken as the uncertainty in the gradient of the line of regression, i.e., $dU_i/d(\Delta P_i/L)$, multiplied by μ_i as given by *Taylor* [1997, chap. 8]. Further details of the uncertainty analysis are provided in the supporting information (Text S2).

3. Capillary Tube Model and Equivalent Slip Length

We translate enhanced permeability into an equivalent slip length by modeling the porous medium as a capillary tube of radius $r_1 = 5\sqrt{k/\phi}$ [*Dullien*, 1991], with the defending phase (water during oil injection and oil during waterflood) distributed as an immobile, thin annular film on the tube wall and the injected fluid flowing through the middle (Figure 1). This approximation is reasonable even where the defending phase is the nonwetting phase provided that its saturation is small. Such films have been captured on grain surfaces in mixed-wet porous media during and after waterflood using X-ray microcomputed tomography (micro-CT) [*Iglauer et al.*, 2012; *Singh et al.*, 2016] and lab-on-a-chip methods [*Bowden et al.*, 2016], although it is not possible to determine from the images whether the oil was immobile. However, it is reasonable to assume that if no further oil was produced as water was injected, the remaining oil within the sample was immobile. Similarly, water was not produced during oil injection after initial oil saturation was established, which indicates that the connate water was immobile.

The volumetric flow rate for steady flow through a circular tube of radius R is given by the classic Poiseuille solution as

$$Q_i = \frac{\pi}{8\mu_i}\frac{\Delta P_i}{L}R^4. \tag{3}$$

At 100% brine saturation, the brine flows through the entire cross section and $R = r_1$. During oil injection at S_{oi}, the connate water is assumed to form a film of thickness $r_1 - r_2$, where $r_2 = r_1\sqrt{S_{oi}} \leq r_1$. At residual oil saturation, $r_2 = r_1\sqrt{1 - S_{or}} \leq r_1$ (Figure 1). In the absence of any enhancement of permeability, the injected fluid flows through a cross-sectional area of radius $R = r_2$ and

$$k_{ri} = \frac{Q_i(R = r_2)}{Q_i(r_1)} = \left(\frac{r_2}{r_1}\right)^4 = S_i^2, \tag{4}$$

where S_i is the saturation of the flowing phase i.

Additional enhancement of relative permeability beyond that associated with the reduced radius available to flow is accounted for by taking $R = r_2 + \delta_i$, where δ_i is an equivalent slip length (Figure 1). The relative

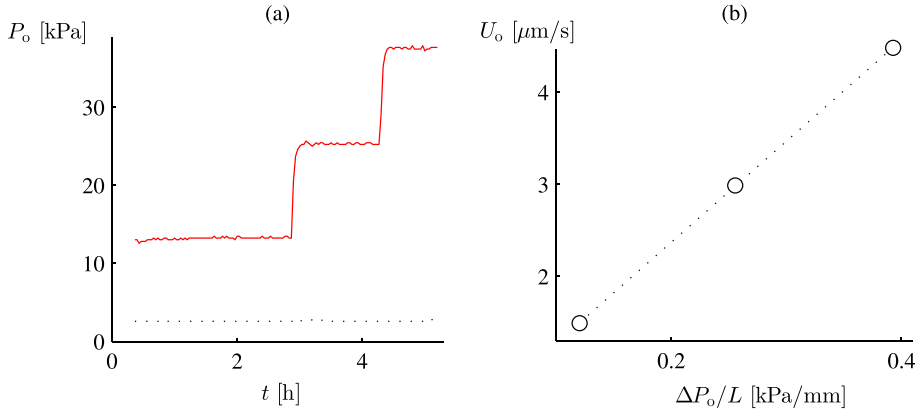

Figure 2. (a) Pressure at the upstream (solid line) and downstream (dotted) ends of Indiana limestone M as a function of time as oil injection velocity, U_o, was increased in discrete intervals and (b) the corresponding time-averaged pressure drop per unit length as a function of U_o during oil permeability measurement. The standard deviation of the pressure measurements over time are plotted as vertical bars in Figure 2b, but they are smaller than the size of the markers and are thus not visible.

permeability during oil/brine flow is then the relative change in Q between the single-phase flow with no slip and two-phase flow with slip:

$$k_{ri} = \frac{Q_i(r_2 + \delta_i)}{Q_i(r_1)} \approx \frac{r_2^4 + 4r_2^3\delta_i}{r_1^4}; \tag{5}$$

the last term was derived by assuming $\delta_i \ll r_2$. We use equation (5) to translate measured values of (k_{ro}, k_{rw}) into equivalent lengths (δ_o, δ_w).

4. Results and Discussion

Of 20 k, 14 $k_o(S_{oi})$, and 19 $k_w(S_{or})$ measurements, seven were discarded because the pressure readings did not stabilize (Table S2). Among the remaining 46 permeability measurements, the pressure drop across the length of the core increased linearly with U_i where multiple injection velocities were considered at steady state, validating the use of equation (2) to calculate k_i (e.g., Figures 2 and S3 to S5).

4.1. Relative Permeability

Figure 3 presents (a) k_{ro} at S_{oi} and (b) k_{rw} at S_{or} normalized by S_i^2. Also included are analogous measurements on Torpedo sandstone by *Owens and Archer* [1971]. (Experimental studies investigating the systematic impact of contact angle on relative permeability are limited, and if we constrain our selection to studies where a sample was rendered mixed wet during primary drainage by surface active components in the oil phase, and where the saturation and wettability history are unambiguous, we retain the data of *Owens and Archer* [1971] only.) From equation (4), $k_{ri}/S_i^2 = 1$ if the only contribution of the defending phase was to reduce the cross-sectional area available to the injected phase to flow. $k_{ro}(S_{oi})/S_{oi}^2$ decreases and $k_{rw}(S_{or})/\left(1 - S_{or}\right)^2$ increases with increasing θ_w over the full range of $\theta_w (> 50°)$ considered in all three limestones (Figure 3). These trends are consistent with measurements in Torpedo sandstone reported by *Owens and Archer* [1971] (Figure 3, crosses), suggesting that they are salient features of mixed-wet rock.

The global negative and positive correlations of $k_{ro}(S_{oi})$ and $k_{rw}(S_{or})$, respectively, with θ_w are attributed to the oil and brine preferentially occupying smaller and larger pores, respectively, as θ_w increases. The continuous nature of the variation—instead of a sharp transition at a single value of contact angle in the vicinity of $\theta_w \approx 90°$ where the oil becomes the wetting phase—is attributed to the wide distribution of in situ contact angles expected within the pore space of the rocks arising from variations in local pore geometry, exposure to oil, mineralogy, and grain roughness—all of which affect the local contact angle. Indeed, local static contact angles have been found to be normally distributed with a standard deviation of $\pm 15°$ in a homogeneous limestone at its natural, water-wet state [*Scanziani et al.*, 2017]. Presumably, an increasing fraction of the grain surface is oil wetting as θ_w increases.

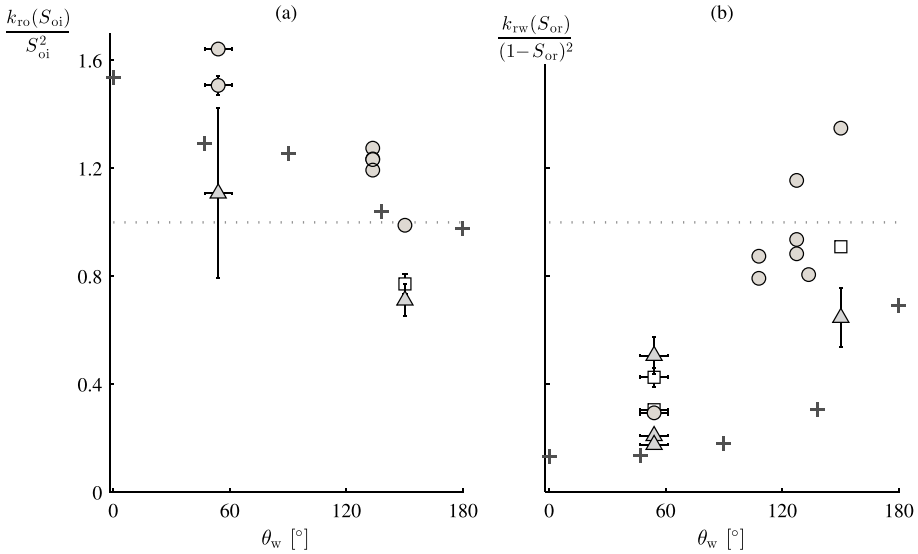

Figure 3. Saturation-normalized (a) oil relative permeability at initial oil saturation and (b) brine relative permeability at residual oil saturation as a function of contact angle for Indiana (circle), Guiting (square), and Estaillades limestones (triangle) from the present study and for Torpedo sandstone as measured by *Owens and Archer* [1971] (crosses). Each marker represents a single experiment. Horizontal bars depict the standard error of the mean over replicate measurements; vertical bars depict uncertainty in k and k_j measurements (cf. supporting information).

Irrespective of θ_w and the flowing phase, k_{ri}/S_i^2 is largest for Indiana limestone (Figure 3, circle) and smallest for Estaillades limestone (triangle). This trend is attributed primarily to differences in the pore size. Previously, water permeability enhancement between two hydrophobic plates has been shown to decrease with increasing distance between the plates [*Lee et al.*, 2007]. Similarly, k_{ri} data compiled by *Berg et al.* [2008] broadly decrease with increasing equivalent capillary radius, r_1 $\left(=5\sqrt{k/\phi}\right)$. By analogy, we may expect that Estaillades limestone, whose equivalent capillary radius of $r_1 = 3.9 \pm 0.5\mu m$ is a factor of 4 larger than that of Indiana limestone ($r_1 = 1.1 \pm 0.2$ μm) and 1 order of magnitude larger than that of Guiting limestone ($r_1 = 320 \pm 80$ nm), may display lower relative permeabilities. The physical mechanisms responsible for this trend, however, have not been conclusively established in the literature and are beyond the scope of the present study. Further insight requires additional measurements in different rocks.

4.2. Apparent Slip

Enhanced permeability is observed for both phases. $k_{ro}(S_{oi})/S_{oi}^2 > 1$ at $\theta_w < 140°$ under conditions considered presently, i.e., $S_{oi} \geq 0.8$. In contrast, $k_{rw}(S_{or})/(1-S_{or})^2 > 1$ only in Indiana limestone at $\theta_w = 150°$. Combined, at least for the rocks considered presently, advancing contact angle of $\theta_w = 140°$ appears to be a critical threshold for the onset of enhanced permeability. $\theta_w = 140°$ corresponds to a static contact angle of $0.877\theta_w = 120°$ according to the empirical model by *Morrow* [1975] (Class II). Remarkably, this value coincides with the threshold for water flowing between a pair of smooth, uniformly oil-treated hydrophobic plates at the limit of zero residual oil: the drag exerted by such flows does not display any θ_w dependence for static contact angles of 110° but decreases for static contact angles above 120° [*Lee et al.*, 2007; *Watanabe et al.*, 1999]. While enhanced gas permeability has been observed in gas/liquid/rock systems [*Richardson et al.*, 1952; *Oak et al.*, 1990; *Dana and Skoczylas*, 1999; *Pini and Benson*, 2013; *Alizadeh and Piri*, 2014], its wettability dependence cannot be discerned as contact angles were not varied and $\theta_g \approx 140°$ in all gas/liquid pairs considered.

Figure 4 presents the equivalent slip length, δ_i, as a function of the advancing contact angle as measured through the flowing phase, θ_i. At all θ_i, $\delta_w < \delta_o$. In the present study, the water saturation at which end point brine permeability was measured falls within $0.55 < S_w \leq 0.81$ (Table S2); the relatively low saturation of the flowing phase may account for the absence of slip during water injection.

The maximum equivalent slip length was 170 nm and is up to 2 orders of magnitude larger than the molecular size of the organic acids (Table S3). Slip has previously been correlated to molecular properties, such as the

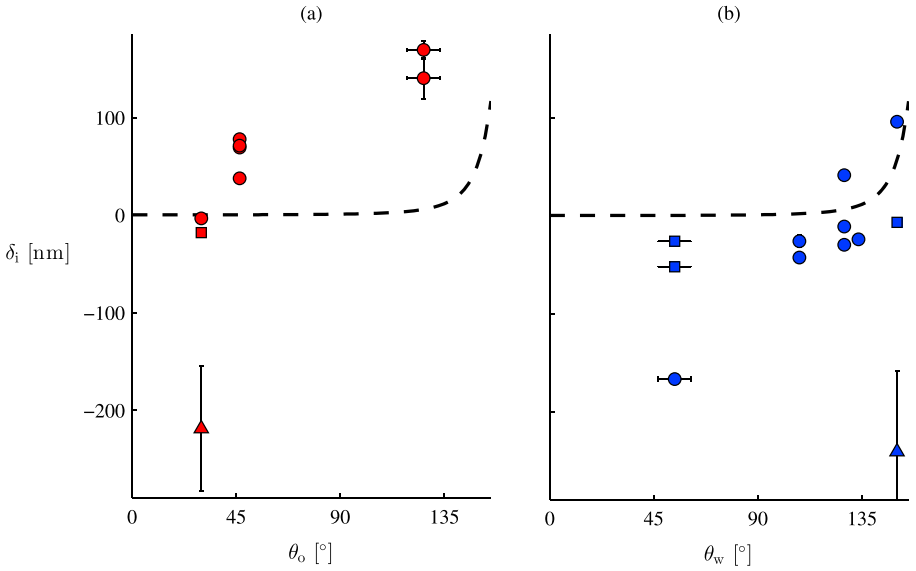

Figure 4. Equivalent slip length (equation (5)) as a function of the contact angle as measured through the flowing phase for (a) oil and (b) brine. Dashed line is the scaling $\delta_i = (1 + \cos\theta_i)^{-2}$ proposed by *Huang et al.* [2008]. The uncertainty in k and k_i is depicted by vertical bars; where they are not visible, they are smaller than the marker size. There are data points for Estaillades limestone at $\theta_w = 54°$, $\delta_w = -688 \pm 8$ and -590 ± 9 nm which are not visible in the figure. Estaillades G is excluded because the large uncertainty in k results in an uncertainty in slip length that exceeds the magnitude of δ_o (Table S2).

number of monomers in a chain [*de Gennes*, 1979], itself correlated to the kinetic diameter. The physically based scaling $\delta_i \propto (\cos\theta_i + 1)^{-2}$ proposed by *Huang et al.* [2008] underpredicts the slip length by 1 to 2 orders of magnitude. However, slip lengths of the same order of magnitude have been measured previously for hexadecane on smooth surfaces that are both wetting and nonwetting to the flowing liquid [*Pit et al.*, 2000]. At the same time, our results are smaller than slip lengths on the order of microns reported on, e.g., silanized glass [*Tretheway and Meinhart*, 2002]. This discrepancy is attributed to roughness on the grain surface associated with naturally occurring grooves and microporosity; different types of nanometer-scale roughness have been shown to inhibit slip [*Pit et al.*, 2000; *Zhu and Granick*, 2002]. A second plausible explanation for the discrepancy is the finite water saturation at which the rocks were equilibrated with the acid-containing oil phase prior to oil permeability measurements. The connate water gives rise to differential adsorption of surface active components in the oil phase, which has been found to suppress slip on macroscopically smooth surfaces [*Pit et al.*, 2000]. Further insight requires additional measurements on rock-rendered mixed wet at a range of oil saturations.

4.3. Limitations of the Analysis

The present analysis is based on the approximation of the pore space as a bundle of identical circular capillary tubes. This model may be expanded to include different geometries as informed by, e.g., micro-CT scans of the pore space of the rock [e.g., *Øren et al.*, 1998; *Valvatne and Blunt*, 2004]. Unfortunately, a significant portion of the pore space of the limestones considered presently falls below the typical voxel size of commercial micro-CT scans [*Tanino and Blunt*, 2012; *Gharbi and Blunt*, 2012] and the extraction of a representative pore network for these rocks remains a challenge. Indeed, bundle-of-tube models continue to be widely used to represent the pore space of rock [e.g., *Holm et al.*, 2010; *Li et al.*, 2017; *Xu et al.*, 2016]. Thus, the extension of the capillary tube model to complex geometries or a combination of geometries is a topic for future work.

One alternative to the present model is to assume that every capillary tube is occupied by one fluid only and that the oil and brine occupy different tubes. With this fluid distribution, $k_{ri} = S_i$ if the only contribution of the defending phase is to reduce the cross-sectional area available to the injected fluid [*Tanino and Blunt*, 2013]; i.e., apparent slippage corresponds to $k_{ri} > S_i$. In the experiments considered presently, $k_{ro}/S_o > 1$ in all cores at $\theta_w < 140°$. Thus, even with this more severe criterion, apparent slippage at initial oil saturation is found to occur at $\theta_w < 140°$.

5. Conclusions

Laboratory measurements of oil/brine permeability of limestones partially saturated with water, whose grain surfaces were rendered oil wet (hydrophobic) to different degrees by in situ adsorption of organic acids of different alkyl chain length in the oil phase, were presented. Unlike most studies in the literature on slippage, the wettability of the solid surface (grain surface here) is heterogeneous at the pore scale and subpore scale and the surface is porous due to microporosity. The saturation-normalized relative permeability of oil and brine, k_{ri}/S_i^2, increases as the grain surface in the rock becomes less wetting to that phase. The enhanced permeability to one fluid cannot be explained by the decrease in cross-sectional area available to flow due to the presence of a second fluid. In particular, $k_{ri}/S_i^2 > 1$ at $\theta_w < 140°$ in all rock considered, yielding equivalent slip lengths of up to 170 nm. The equivalent slip lengths decrease with increasing mean pore radius amongst the three limestones considered presently. In recent literature, slip has predominantly been associated with the flow of nonwetting fluid against a surface [*Berg et al.*, 2008; *Tretheway and Meinhart*, 2002; *Huang et al.*, 2008]. The present results demonstrate that on the contrary, the flowing phase is not required to be the nonwetting phase for enhanced permeability, or apparent slip, to occur in mixed-wet rock.

Acknowledgments
This material includes work supported by a Society of Petrophysicists and Well Log Analysts Foundation grant and an Aberdeen Formation Evaluation Society scholarship. M.C. was supported by a University of Aberdeen College of Physical Sciences studentship. The authors gratefully acknowledge Amer Syed for his assistance with the assembly and maintenance of the coreflood rigs, Jim Anderson for helpful discussions, and the two anonymous reviewers for their comments and suggestions. All data used in this study will be made available from the corresponding author upon request.

References

Al-Gharbi, M. S., X. Jing, M. Kraaijveld, J. B. Hognestad, and P. O. Udeh (2007), SCAL relative permeability measurements and analyses for a cluster of fields in South Oman, paper presented at International Petroleum Technology Conference, Dubai, UAE, 4–6 Dec., doi:10.2523/IPTC-11415-MS.

Alizadeh, A., and M. Piri (2014), The effect of saturation history on three-phase relative permeability: An experimental study, *Water Resour. Res.*, *50*(2), 1636–1664.

Bäumchen, O., and K. Jacobs (2010), Can liquids slide? Linking stability and dynamics of thin liquid films to microscopic material properties, *Soft Matter*, *6*(24), 6028–6035.

Berg, S., A. W. Cense, J. P. Hofman, and R. M. M. Smits (2008), Two-phase flow in porous media with slip boundary condition, *Transp. Porous Media*, *74*(3), 275–292.

Bowden, S. A., Y. Tanino, B. Akamairo, and M. Christensen (2016), Recreating mineralogical petrographic heterogeneity within microfluidic chips: Assembly, examples, and applications, *Lab Chip*, *16*, 4677–4681, doi:10.1039/C6LC01209D.

Burdine, N. T. (1953), Relative permeability calculations from pore size distribution data, *J. Petrol. Technol.*, *5*(3), 71–78, doi:10.2118/225-G.

Choi, C.-H., and C.-J. Kim (2006), Large slip of aqueous liquid flow over a nanoengineered superhydrophobic surface, *Phys. Rev. Lett.*, *96*(6), 066001, doi:10.1103/PhysRevLett.96.066001.

Choi, C.-H., K. J. A. Westin, and K. S. Breuer (2003), Apparent slip flows in hydrophilic and hydrophobic microchannels, *Phys. Fluids*, *15*(10), 2897–2902, doi:10.1063/1.1605425.

Christensen, M., and Y. Tanino (2017), Waterflood oil recovery from mixed-wet limestone: Dependence on contact angle, *Energy Fuel*, *31*(2), 1529–1535, doi:10.1021/acs.energyfuels.6b03249.

Churaev, N., V. Sobolev, and A. Somov (1984), Slippage of liquids over lyophobic solid surfaces, *J. Colloid Interface Sci.*, *97*(2), 574–581, doi:10.1016/0021-9797(84)90330-8.

Cottin-Bizonne, C., A. Steinberger, B. Cross, O. Raccurt, and E. Charlaix (2008), Nanohydrodynamics: The intrinsic flow boundary condition on smooth surfaces, *Langmuir*, *24*(4), 1165–1172, doi:10.1021/LA7024044.

Dana, E., and F. Skoczylas (1999), Gas relative permeability and pore structure of sandstones, *Int. J. Rock Mech. Min.*, *36*(5), 613–625.

de Gennes, P.-G. (1979), Ecoulements viscometriques de polymeres enchevetres, *C. R. Seances Acad. Sci. Ser. B*, *310*(288), 219–220.

Drda, P. P., and S.-Q. Wang (1995), Stick-slip transition at polymer melt/solid interfaces, *Phys. Rev. Lett.*, *75*(14), 2698–2701, doi:10.1103/PhysRevLett.75.2698.

Dullien, F. A. L. (1991), *Porous Media: Fluid Transport and Pore Structure*, 2nd ed., Academic Press, San Diego, Calif.

Gharbi, O., and M. J. Blunt (2012), The impact of wettability and connectivity on relative permeability in carbonates: A pore network modeling analysis, *Water Resour. Res.*, *48*, W12513, doi:10.1029/2012WR011877.

Holm, R., M. I. J. van Dijke, and S. Geiger (2010), Three-phase flow modelling using pore-scale capillary pressures and relative permeabilities for mixed-wet media at the continuum-scale, *Transp. Porous Media*, *81*(3), 423–442, doi:10.1007/s11242-009-9415-0.

Honarpour, M., L. F. Koederitz, and A. H. Harvey (1982), Empirical equations for estimating two-phase relative permeability in consolidated rock, *J. Petroleum Technol.*, *34*(12), 2905–2908, doi:10.2118/9966-PA.

Huang, D. M., C. Sendner, D. Horinek, R. R. Netz, and L. Bocquet (2008), Water slippage versus contact angle: A quasiuniversal relationship, *Phys. Rev. Lett.*, *101*(22), 226101, doi:10.1103/PhysRevLett.101.226101.

Iglauer, S., M. A. Fernø, P. Shearing, and M. J. Blunt (2012), Comparison of residual oil cluster size distribution, morphology and saturation in oil-wet and water-wet sandstone, *J. Colloid Interf. Sci.*, *375*(1), 187–192, doi:10.1016/j.jcis.2012.02.025.

Jerauld, G. (1997), Prudhoe Bay gas/oil relative permeability, *SPE Reservoir Eng.*, *12*(1), 66–73, doi:10.2118/35718-PA.

Joekar-Niasar, V., S. M. Hassanizadeh, and A. Leijnse (2008), Insights into the relationships among capillary pressure, saturation, interfacial area and relative permeability using pore-network modeling, *Transp. Porous Media*, *74*(2), 201–219, doi:10.1007/s11242-007-9191-7.

Joseph, P., C. Cottin-Bizonne, J.-M. Benoît, C. Ybert, C. Journet, P. Tabeling, and L. Bocquet (2006), Slippage of water past superhydrophobic carbon nanotube forests in microchannels, *Phys. Rev. lett.*, *97*(15), 156104, doi:10.1103/PhysRevLett.97.156104.

Lee, H.-B., I. W. Yeo, and K.-K. Lee (2007), Water flow and slip on NAPL-wetted surfaces of a parallel-walled fracture, *Geophys. Res. Lett.*, *34*, L19401, doi:10.1029/2007GL031333.

Li, S., M. Dong, and P. Luo (2017), A crossflow model for an interacting capillary bundle: Development and application for waterflooding in tight oil reservoirs, *Chem. Eng. Sci.*, *164*, 133–147, doi:10.1016/j.ces.2017.01.059.

Lomeland, F., E. Ebeltoft, and W. H. Thomas (2005), A new versatile relative permeability correlation, paper SCA2005-32 presented at International Symposium of the Society of Core Analysts, Toronto, Canada, 21–25 Aug.

Morrow, N. R. (1975), The effects of surface roughness on contact angle with special reference to petroleum recovery, *J. Can. Petrol. Technol.*, *14*(4), 42–53, doi:10.2118/75-04-04.

Oak, M. J., L. E. Baker, and D. C. Thomas (1990), Three-phase relative permeability of Berea sandstone, *J. Petrol. Technol.*, *42*(8), 1054–1061, doi:10.2118/17370-PA.

Øren, P.-E., S. Bakke, and O. J. Arntzen (1998), Extending predictive capabilities to network models, *Soc. Petrol. Eng. J.*, *3*(4), 324–336, doi:10.2118/52052-PA.

Owens, W. W., and D. L. Archer (1971), The effect of rock wettability on oil-water relative permeability relationships, *J. Petrol. Technol.*, *23*(7), 873–878, doi:10.2118/3034-PA.

Pini, R., and S. M. Benson (2013), Simultaneous determination of capillary pressure and relative permeability curves from core-flooding experiments with various fluid pairs, *Water Resour. Res.*, *49*, 3516–3530, doi:10.1002/wrcr.20274.

Pit, R., H. Hervet, and L. Léger (2000), Direct experimental evidence of slip in hexadecane: Solid interfaces, *Phys. Rev. Lett.*, *85*(5), 980–983, doi:10.1103/PhysRevLett.85.980.

Richardson, J., J. Kerver, J. Hafford, and J. Osoba (1952), Laboratory determination of relative permeability, *Pet. Trans. (AIME)*, *4*(8), 187–196.

Ryazanov, A. V., M. I. J. van Dijke, and K. S. Sorbie (2010), Pore-network prediction of residual oil saturation based on oil layer drainage in mixed-wet systems, paper presented at SPE Improved Oil Recovery Symposium, Society of Petroleum Engineers, Oklahoma, USA, doi:10.2118/129919-MS, 24–28 Apr.

Scanziani, A., K. Singh, M. J. Blunt, and A. Guadagnini (2017), Automatic method for estimation of in situ effective contact angle from X-ray micro tomography images of two-phase flow in porous media, *J. Colloid Interface Sci.*, *496*, 51–59, doi:10.1016/j.jcis.2017.02.005.

Singh, K., B. Bijeljic, and M. J. Blunt (2016), Imaging of oil layers, curvature, and contact angle in a mixed-wet and a water-wet carbonate rock, *Water Resour. Res.*, *52*, 1716–1728, doi:10.1002/2015WR0180072.

Tanino, Y., and M. J. Blunt (2012), Capillary trapping in sandstones and carbonates: Dependence on pore structure, *Water Resour. Res.*, *48*, W08525, doi:10.1029/2011WR011712.

Tanino, Y., and M. J. Blunt (2013), Laboratory investigation of capillary trapping under mixed-wet conditions, *Water Resour. Res.*, *49*, 4311–4319, doi:10.1002/wrcr.20344.

Tanino, Y., B. Akamairo, M. Christensen, and S. A. Bowden (2015), Impact of displacement rate on waterflood oil recovery under mixed-wet conditions, paper SCA-A031 presented at International Symposium of the Society of Core Analysts, Society of Core Analysts, St, John's Newfoundland and Labrador Canada.

Taylor, J. R. (1997), *An Introduction to Error Analysis: The Study of Uncertainties in Physical Measurements*, 2nd ed., Univ. Sci. Books, Sausalito, Calif.

Thompson, P. A., and S. M. Troian (1997), A general boundary condition for liquid flow at solid surfaces, *Nature*, *389*(6649), 360–362, doi:10.1038/38686.

Tretheway, D. C., and C. D. Meinhart (2002), Apparent fluid slip at hydrophobic microchannel walls, *Phys. Fluids*, *14*(3), L9–L12, doi:10.1063/1.1432696.

Valvatne, P. H., and M. J. Blunt (2004), Predictive pore-scale modeling of two-phase flow in mixed wet media, *Water Resour. Res.*, *40*, W07406, doi:10.1029/2003WR002627.

Wang, S.-Q., and P. A. Drda (1996), Stick- slip transition in capillary flow of polyethylene: 2. Molecular weight dependence and low-temperature anomaly, *Macromolecules*, *29*(11), 4115–4119, doi:10.1021/MA951512e.

Watanabe, K., Y. Udagawa, and H. Udagawa (1999), Drag reduction of Newtonian fluid in a circular pipe with a highly water-repellent wall, *J. Fluid Mech.*, *381*, 225–238.

Wu, Y., P. J. Shuler, M. Blanco, Y. Tang, and W. A. Goddard III (2008), An experimental study of wetting behavior and surfactant EOR in carbonates with model compounds, *Soc. Petrol. Eng. J.*, *13*(1), 26–34, doi:10.2118/99612-PA.

Xu, W. S., P. Y. Luo, L. Sun, and N. Lin (2016), A prediction model of the capillary pressure J-function, *PLoS One*, *11*(9), 1–9, doi:10.1371/journal.pone.0162123.

Yang, S.-C. (2006), Effects of surface roughness and interface wettability on nanoscale flow in a nanochannel, *Microfluid. Nanofluid.*, *2*(6), 501–511, doi:10.1007/s10404-006-0096-5.

Zhu, Y., and S. Granick (2002), Limits of the hydrodynamic no-slip boundary condition, *Phys. Rev. Lett.*, *88*(10), 106102, doi:10.1103/PhysRevLett.88.106102.